IOP Publishing Superconductor Science and Technology
Supercond. Sci. Technol. 31 (2018) 085010 (12pp) https://doi.org/10.1088/1361-6668/aad00c

Thermal stability and mechanical behavior in no-insulation high-temperature superconducting pancake coils

Donghui Liu[1,2], Weiwei Zhang[1,2], Huadong Yong[1,2,3] and Youhe Zhou[1,2,3]

[1] Key Laboratory of Mechanics on Disaster and Environment in Western China, Ministry of Education of China, Lanzhou University, Lanzhou, Gansu 730000, People's Republic of China
[2] Department of Mechanics and Engineering Sciences, College of Civil Engineering and Mechanics, Lanzhou University, Lanzhou, Gansu 730000, People's Republic of China

E-mail: yonghd@lzu.edu.cn and zhouyh@lzu.edu.cn

Received 4 December 2017, revised 20 May 2018
Accepted for publication 29 June 2018
Published 17 July 2018

Abstract

No-insulation (NI) high-temperature superconducting (HTS) coils exhibit high thermal stability and self-protecting features compared with traditional insulated HTS coils. As NI coils experience heat disturbance, the underlying mechanism of the heat propagation, the changes of the central field and voltage of the coil need to be further explored. Moreover, due to the rapid temperature rise caused by the heat disturbance, the coil typically suffers from large strain and stress. Therefore, the mechanical behavior is also a vital factor in the design and operation of superconducting magnets. This paper proposes a multiphysics quench model to study the thermal stability, composed of an equivalent circuit axisymmetric model combined with a two-dimensional magnetic field model and a one-dimensional (1D) heat transfer model. An additional 1D solid mechanical model is used to analyze the mechanical behavior of the NI coil. The results indicate that when the temperature of the coil exceeds its critical value, the current flows along the radial direction. The heat generated by the radial resistance of the coil is small, so that it is difficult to induce a quench. The thermal expansion and heat propagation velocity also affect the distributions of the hoop and radial stresses in the coil. The change of the hoop stress is larger than that of the radial stress, and the electromagnetic force has a relatively small effect in the self-field. The pulsed energy, inner diameter of the coil and location of the heater are all found to have an observable effect on the thermal stability and mechanical behavior.

Keywords: no-insulation coil, quench model, temperature, strain and stress

(Some figures may appear in colour only in the online journal)

1. Introduction

Due to the high critical current density in the high-field, high-temperature superconductors (HTS) are a promising candidate for the development of high-field magnets [1–3]. It is well known that quench detection and protection for HTS magnets are still a severe challenge because of the low quench propagation velocity [4–8]. A no-insulation (NI) approach with no turn-to-turn insulation between adjacent turns was proposed for the design of high-field DC magnets in 2011 [9]. This means that the current can flow along the radial direction in the coil. To be more specific, when a local hotspot or local defect appears in the coil, the lower radial resistivity allows the current to bypass it [10–13]. Moreover, unlike an insulated coil, an NI coil does not burn out under an overcurrent, which is twice as large as the critical current [9, 14, 15]. Recently, NI coils with high thermal stability and self-protecting features have been widely studied to provide guidelines for the potential design of magnets in the future [10, 12, 15–19].

Although an NI coil is more stable than an insulated coil, it is still possible to induce a quench for the heat disturbance

[3] Authors to whom any correspondence should be addressed.

and overcurrent [20, 21]. To facilitate the development of high-field magnets composed by NI coils, the thermal stability under a large-sized heat disturbance needs to be further investigated. Many previous studies have focused on the thermal stability and self-protecting features of NI coils under local heat disturbance [10, 12, 15, 22–24], but a few studies have taken the mechanical behavior into consideration [25]. In addition, it is difficult to monitor the redistribution of current and heat propagation in the whole coil experimentally. Thus, a multiphysics quench model that can analyze the thermal stability and mechanical behavior of the NI coil is necessary to force the application of high-field NI magnets.

At present, the equivalent circuit model is an effective method to calculate the distribution of current during heat disturbance and the charging and discharging processes [10, 12, 26–29]. Based on local heat disturbance and local electrical contact resistance between turns in the NI coil, the equivalent circuit grid model and partial element equivalent model were used to simulate the distribution of the temperature and current [10, 12]. The self-protecting features in the NI coil were clarified in detail and the transient electromagnetic and thermal behaviors were studied as well. It is to be noted that the thermal stability and mechanical behavior of the coil under heat disturbance of the whole turn has not been thoroughly analyzed and the underlying mechanisms need to be further studied. In this case, the equivalent circuit axisymmetric model is suitable for analyzing the redistribution of the current during heat disturbance. In addition, the equivalent circuit axisymmetric model has already been developed to the extent that it can calculate the distribution of the current [28, 29].

In this paper, a multiphysics quench model is built by combining an equivalent circuit axisymmetric model with a 2D magnetic field model and a 1D heat transfer model. The quench model can obtain the distributions of the current and temperature, which can further clarify the thermal stability under heat disturbance. Moreover, the radial resistivity is related to the mechanical behavior [25, 30], and the strain has been successfully used to detect the quench [31, 32]. Since the distributions of strain and stress during the heating and recovery processes have not previously been taken into consideration, we also develop a 1D solid mechanical model to discuss the changes of strain and stress in the paper. In section 2, the multiphysics quench model and 1D solid mechanical model are described in detail. The thermal stability and mechanical behavior are analyzed in section 3. Section 4 discusses the potential effect of the main factors on the distributions of temperature, central field, coil voltage, radial and hoop stresses. The conclusions in the paper are summarized in the final section.

2. Model descriptions

2.1. Equivalent circuit axisymmetric model

Due to the NI between turns, the current can be shared along the radial and azimuthal directions of the coil. Figure 1 shows a schematic illustration of the equivalent circuit axisymmetric model for a single-pancake NI coil. Note that the circuit model is not perfect. However, because the heat generated by the low contact resistance is very small, the temperature distribution is mainly determined by the local heat disturbance. Moreover, the mechanical behavior is mainly affected by the change of temperature due to the small electromagnetic force. By comparing two different circuit models (the other model is where the nth turn has an independent bypass circuit, which leads to a large contact resistance in total), it can be seen that the effect of the bypass circuit between the $(n-1)$th and nth turns on the mechanical stresses can be neglected in the simulation. The azimuthal current is a combination of the currents of the superconducting layer and normal layers, and the radial current flows through the turn-to-turn contact resistance. For each turn, the governing equations can be derived from Kirchhoff's current and voltage laws at each circuit node and circuit loop:

$$\begin{cases} I_{op} = i_m + j_m \\ u_m - j_m R_{r,m} = 0 & m < N-1, \\ u_m + u_{m+1} - j_m R_{r,m} = 0 & m = N-1 \end{cases} \tag{1}$$

where I_{op}, i_m and j_m are the power supply current, azimuthal current and radial current in the mth turn, respectively. u_m is the voltage across the mth turn circuit and $R_{r,\mathrm{m}}$ is the equivalent turn-to-turn resistance of the mth turn. Because the radial current flows along the transverse direction of the conductor, the equivalent turn-to-turn resistance includes the transverse resistance and turn-to-turn contact resistance of the HTS tape [12, 33],

$$R_{r,\mathrm{m}} = \frac{\rho_r}{S_m}, \tag{2}$$

where S_m is the surface area of the mth turn, and ρ_r represents the equivalent radial contact resistivity, which has been found by experiment to be typically $70\,\mu\Omega\,\mathrm{cm}^2$ at 77 K [13]. The voltage u_m across the mth turn is the sum of the inductive and resistive voltages and is given by:

$$u_m = \sum_{l=1}^{N} M_{\mathrm{m},l}\frac{di_l}{dt} + V_{sc,m}(i_m, I_{c,m}), \tag{3}$$

where $M_{m,l}$ represents the mutual inductance and self-inductance. The inductance of the model can be calculated by implementing a quadruple integral method based on the Neumann formula [10]. $V_{sc,m}$ represents the voltage of the superconducting layer of the mth turn, which depends on the azimuthal current, critical current and temperature of the mth turn. It can be obtained from the following relationships [12, 33],

$$\begin{cases} V_{sc,m} - (i_m - i_{sc,m})R_{n,m} = 0 \\ V_{sc,m} = i_{sc,m}R_{sc,m} \\ R_{sc,m} = \dfrac{E_c l_m}{I_{c,m}}\left(\dfrac{i_{sc,m}}{I_{c,m}}\right)^{n-1} \\ R_{n,m} = \rho_n \dfrac{l_m}{S} \\ I_{c,m} = I_c(T_\mathrm{m})I_c(B_{\parallel,m}, B_{\perp,m}) \end{cases}, \tag{4}$$

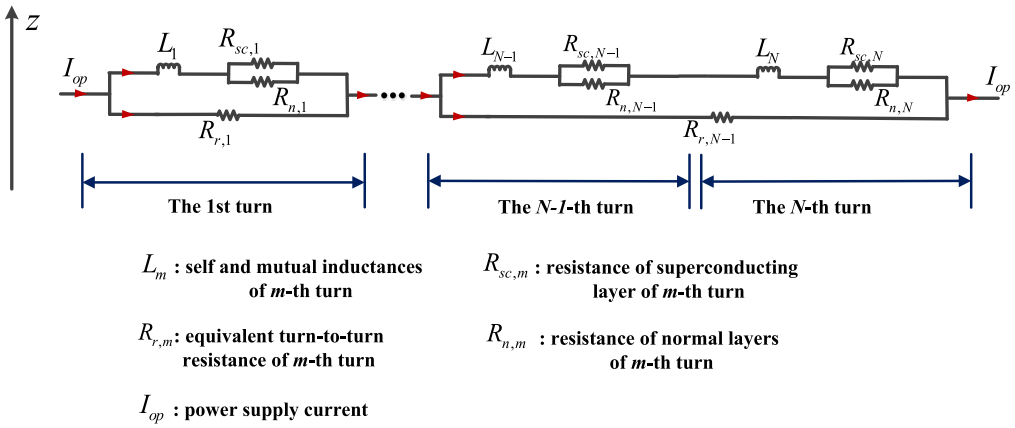

Figure 1. Schematic diagram of the equivalent circuit axisymmetric model for a single-pancake NI coil.

where $i_{sc,m}$, l_m and $I_{c,m}$ represent the current of the superconducting layer, length and critical current of the mth turn. S is the cross-sectional area of the conductor. The temperature-dependent ρ_n obtained by the parallel rule of mixtures is the equivalent resistivity of the normal layers [12, 34]. $R_{n,m}$ and $R_{sc,m}$ are the resistances of the normal layers and superconducting layer of the mth turn composed of two parallel resistances, as shown in figure 1. The n-value is 31 [12] and the critical electrical field E_c is 1 μV cm^{-1} [12, 33]. Note that the bottom equation in (4) represents the critical current being dependent on the temperature and magnetic field. Thus, the critical current $I_{c,m}$ can be obtained from the magnetic field and temperature of the mth turn. The I_{c0} is 220 A, which represents the critical current of the tape at the self-field and 77 K [12, 33].

The temperature-dependent critical current in equation (4) is expressed as [35],

$$I_c(T) = \begin{cases} I_{c0}\dfrac{T_c - T}{T_c - T_0} & \text{if} \quad T < T_c \\ 0 & \text{if} \quad T \geqslant T_c \end{cases}, \tag{5}$$

where the operating temperature T_0 and critical temperature T_c are 77 and 92 K, respectively.

The field-dependent critical current in equation (4) is expressed as [36],

$$I_{c,m}(\mathbf{B}) = \frac{1}{[1 + \sqrt{(kB_{\|})^2 + B_{\perp}^2}/B_c]^b}, \tag{6}$$

where $B_{||}$ and $B_{\perp}$ represent the components of the magnetic field parallel and perpendicular to the surface of the tape, respectively. The parameters k, b and B_c are 0.0605, 0.7580 and 103 mT, respectively [12, 33].

2.2. 2D axisymmetric magnetic field model

After the distribution of the current is obtained by the equivalent circuit axisymmetric model, a 2D axisymmetric magnetic field model can be used to calculate the magnetic field of the coil. In the simulation, the cross-section of the coil is divided into many elements. For a 2D axisymmetric problem, the magnetic field has only two components along the direction of the r and z axes according to the Biot–Savart Law. The magnetic fields of the element $(r, 0, z)$ are expressed as [29],

$$B_r = -\frac{\mu_0}{2\pi}\left(\frac{i_m}{w}\right) \times \int_0^w \int_0^{\pi} \frac{R(z - z_1)\cos\theta d\theta dz_1}{[r^2 + (z - z_1)^2 + R^2 + 2rR\cos\theta]^{3/2}}$$
$$B_z = \frac{\mu_0}{2\pi}\left(\frac{i_m}{w}\right) \times \int_0^w \int_0^{\pi} \frac{R(R + r\cos\theta)d\theta dz_1}{[r^2 + (z - z_1)^2 + R^2 + 2rR\cos\theta]^{3/2}}, \tag{7}$$

where R is the distance between the z axis and each element, θ is the angle between any point of the coil and the r-axis in the $rO\theta$ plane of the cylindrical coordinates, and w is the width of the tape. Here, the azimuthal current i_m is assumed to be uniformly distributed at the cross-section for each turn. Once the magnetic field is obtained, it is fed back to the equivalent circuit axisymmetric model to calculate the critical current of each turn in equation (6).

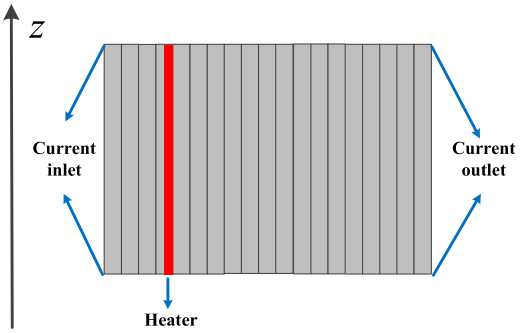

Figure 2. Homogeneous thermal model with the heater.

2.3. Homogeneous thermal model

The tape, which is 4 mm wide and 0.1 mm thick, is treated with a homogeneous equivalent model [12, 33]. Thus, a homogeneous axisymmetric thermal model is used to calculate the distribution of temperature, as shown in figure 2. A heater, which is half the thickness of the tape, is located in

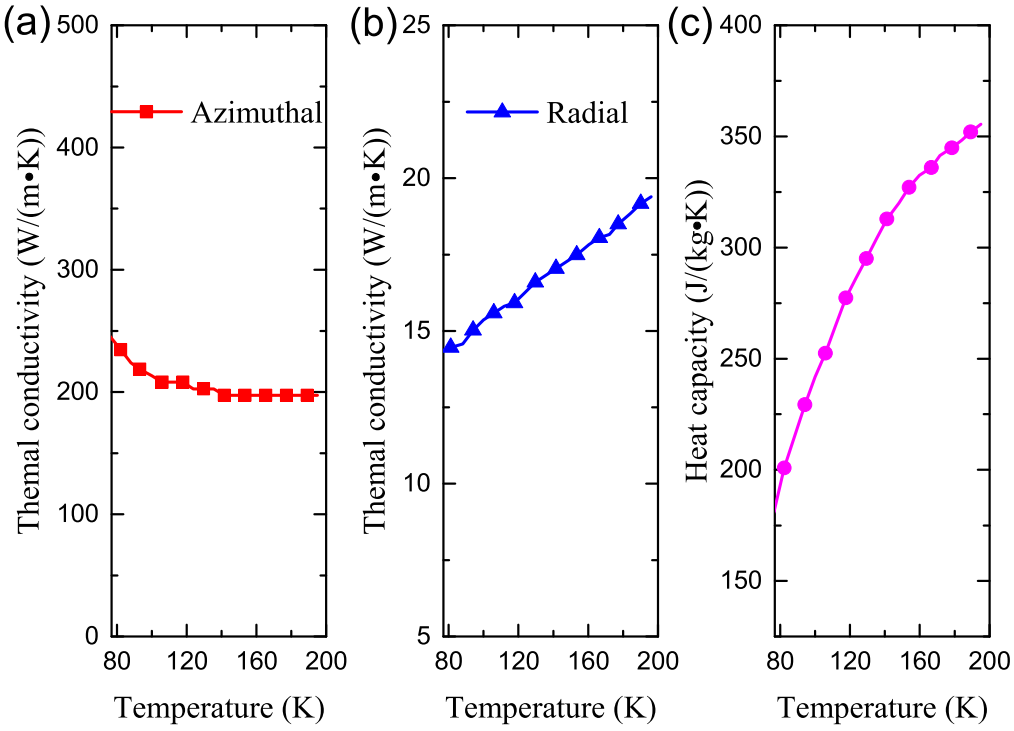

Figure 3. Homogeneous equivalent thermal parameters [12]: (a) azimuthal thermal conductivity, (b) radial thermal conductivity and (c) heat capacity.

turn 4 and is pulsed with energy for 40 ms [12]. Note that the location of the heater in the simulation remains unchanged unless stated otherwise. Moreover, the effective homogeneous parameters are obtained by the rule of mixtures [37], and they have been obtained in [12], as shown in figure 3. It should be pointed out that only the radial thermal conductivity is used in the 1D heat transfer model.

Each pancake is separated by a thick fiber-reinforced plastic plate in the magnet [28, 38]. The heat exchange with the cryogen at the upper and bottom boundaries of the coil is neglected in the simulation. Thus, we only consider the Joule heat diffusing radially at the inner and outer boundaries. The governing equations and cooling boundary conditions of the homogeneous thermal model are given as,

$$\begin{cases} dC\dfrac{\partial T}{\partial t} + \nabla\cdot(-k\nabla T) = \rho_n(T)\left(\dfrac{i_m - i_{sc,m}}{S_c}\right)^2 + \rho_r\delta(r-r_j)\left(\dfrac{j_m}{S_k}\right)^2 + Q_{\text{heat}} & \text{in } \Omega \\ \mathbf{n}\cdot(-k\nabla T) = h(T-T_0) & \text{on } \partial\Omega \end{cases}, \tag{8}$$

where d, C, k and Q_{heat} represent the density, heat capacity, thermal conductivity and pulsed energy generated by the heater, respectively. T is the temperature and t is the time. The heat transfer coefficient h for the convection between the liquid nitrogen bath and superconductor is approximately 400 W $(\text{m}^2\ \text{K})^{-1}$ [39]. The azimuthal current i_m and radial current j_m are obtained by the equivalent circuit axisymmetric model. Because of the radial Joule heat generated in the internal turn-to-turn contact surface r_j (the location of contact surface), the delta function $\delta(r - r_j)$ is introduced to deal with it [40]. The finite difference method is used to solve the equation. Thus, the delta function $\delta(r - r_j)$ is replaced by a discrete approximation $d^{(1)}_{\Delta r}$ and is expressed as [40],

$$d^{(1)}_{\Delta r}(r-r_j) = \begin{cases} (\Delta r - |r-r_j|)/\Delta r^2, & |r-r_j| \leqslant \Delta r \\ 0, & \text{otherwise} \end{cases}, \tag{9}$$

where Δr is the space step of the finite difference method.

2.4. Solid mechanical model

The strain has proved to be an effective method to detect the quench [31, 32]. Moreover, the mechanical behavior has an impact on the turn-to-turn contact resistivity [25, 30]. To understand the variation of the stress and strain in the coil, a 1D solid mechanical model is built that takes the change of temperature into consideration. The outer boundary of the coil is free and the constraints on the inner boundary are discussed in section 3. The governing equations are expressed as [41],

$$d\frac{\partial^2 u}{\partial t^2} = \frac{\partial \sigma_r}{\partial r} + \frac{\sigma_r - \sigma_\varphi}{r} + J_\varphi B_z$$
$$u|_{t=0} = 0, \quad \left.\frac{du}{dt}\right|_{t=0} = 0, \quad \sigma_r|_{r=r_2} = 0, \tag{10}$$

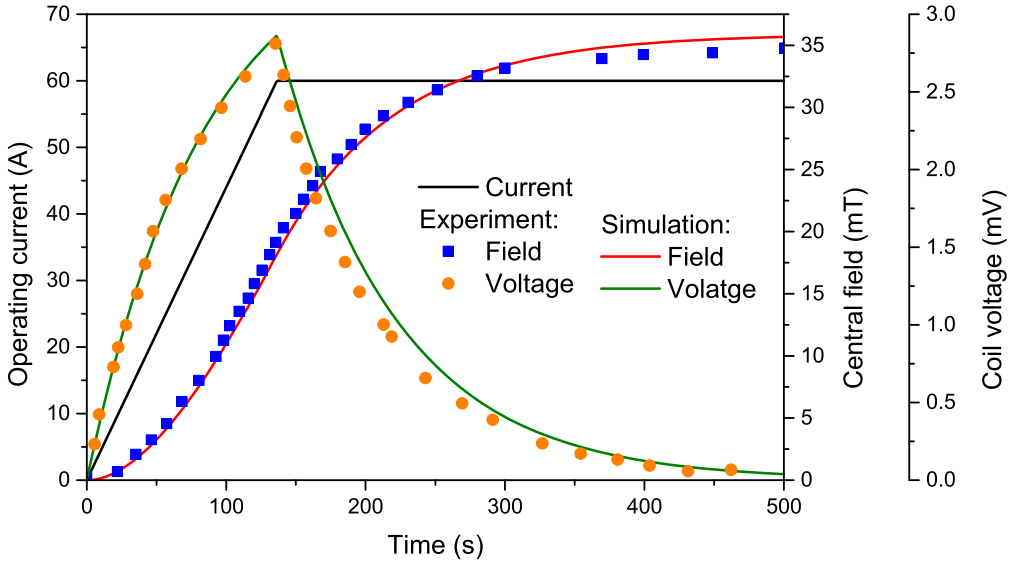

Figure 4. Comparisons of the central field and voltage from experiment and simulation, charging up to 60 A at a rate of 0.44 A s^{-1} in a double-pancake coil.

Table 1. Specification of the single-pancake (SP) NI coil.

Parameters	Coil
Turn number	60
Inner and outer diameters (mm)	100, 112
Height (mm)	4
Thickness of tape (mm)	0.1
Total length of wire (m)	19.9
Inductance, L_{coil} (mH)	0.78
B_z per amp at center (mT)	0.71
Critical temperature T_c (K)	92
I_c coil, @ 77 K (A)	89
I_c tape, @ 77 K (A)	220
Operating current I_{op} (A)	60

where u is the radial displacement. The mechanical model is also solved by the finite difference method, and J_φ and B_z are the azimuthal current density i_m/S (i_m is the azimuthal current and S is the cross-sectional area of the tape) and magnetic field component along the axial direction at each node, respectively. r_2 represents the outer boundary of the coil. According to the geometrical relationship and Hooke's law, the components of strain and stress can be expressed as,

$$\begin{aligned}\varepsilon_r &= \frac{\partial u}{\partial r}, \quad \varepsilon_\varphi = \frac{u}{r}\\ \sigma_r &= \frac{Y_m}{1-\mu^2}(\varepsilon_r + \mu\varepsilon_\varphi) - \frac{Y_m\alpha\Delta T}{1-\mu}\\ \sigma_\varphi &= \frac{Y_m}{1-\mu^2}(\varepsilon_\varphi + \mu\varepsilon_r) - \frac{Y_m\alpha\Delta T}{1-\mu},\end{aligned} \tag{11}$$

where Y_m, μ and α are Young's modulus, Poisson's ratio and thermal expansion coefficient, respectively. Their values obtained by the rule of mixtures are 172 GPa, 0.33 and 13.2×10^{-6} K^{-1} [42, 43]. ΔT is the temperature rise at each node.

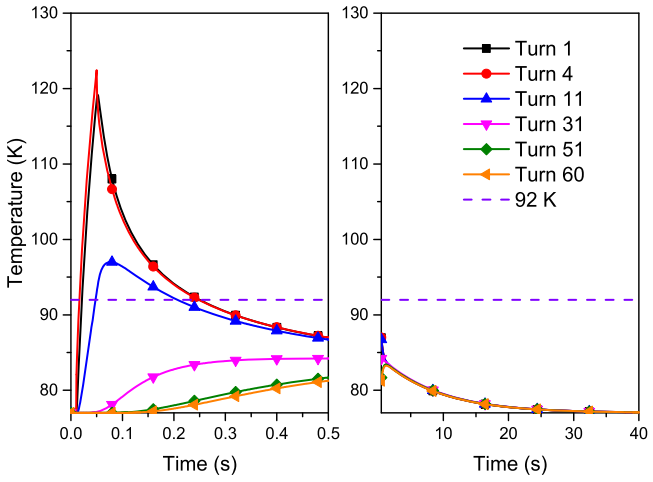

Figure 5. Temperature profile in the 60-turn coil.

3. Results

Table 1 shows many details of the NI coil used in the paper. The heater is located in turn 4 and the pulsed energy Q_{heat} is 75.9 J for a duration of 40 ms. After the coil reaches stable operation, heat disturbance is triggered in the simulation. Thus, the heater is on after 10 ms, so that the coil runs stably.

3.1. Validation of the model and thermal analysis

Here, the central field and voltage from the experiment [26] and simulation are compared by charging up to 60 A at a rate of 0.44 A s^{-1} in a double-pancake coil, as shown in figure 4. The results are in good agreement.

Figure 5 illustrates the temperature distributions in the 60-turn coil. It can be seen that the largest temperature rise happens at the location of the heater. Moreover, the temperature of the outer turns is always lower than the critical temperature in the coil. Therefore, the current of the outer

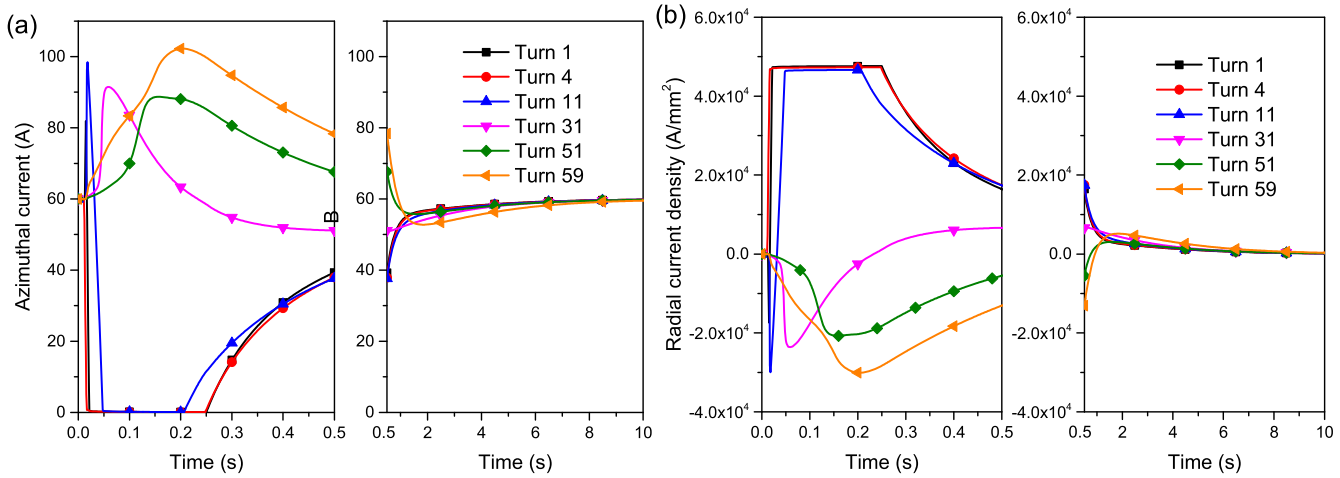

Figure 6. Distributions of azimuthal current (a) and radial current density (b) in the 60-turn coil.

turns can still flow along the azimuthal direction of the coil. Figure 6 shows the repartition of the current. To be specific, when the inner turns quench, the current only flows along the radial direction. At the same time, the current is azimuthally induced in the outer turns, so that the outer turns have large azimuthal current and negative radial current density. Note that the radial current density is defined as in [26].

The central field and coil voltage can dramatically change during the heat disturbance because of the current shared across the radial resistances, as shown in figure 7. The central field decreases to a nonzero value and then starts to recover. The reason is that the current in the outer turns still flows along the superconducting layer during heating, and the heat can be exchanged by the boundaries in time after heating. It can also be found that the attenuation of the central field is mainly dependent on the number of turns exceeding the critical temperature. Moreover, the repartition of the current through the turn-to-turn contact resistances and thermal diffusion process result in a long recovery time for the coil after the local heat disturbance.

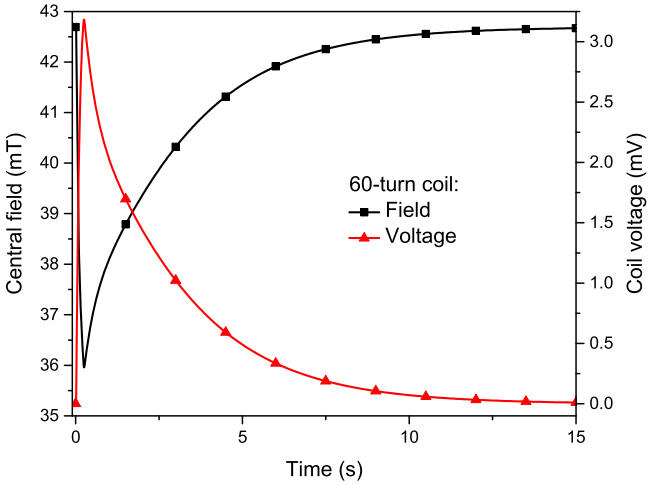

Figure 7. Central field and coil voltage in the 60-turn coil.

3.2. Mechanical behavior

The mechanical behavior plays a vital role in the design and operation of superconducting magnets, but has yet to be analyzed in detail for the heat disturbance and recovery processes. Here, the change of strain and stress will be discussed. In section 2.4, the outer boundary of the coil is free. However, two cases are considered for the inner boundary. For case 1, when the innermost turn of the coil is attached to the inner support structure using adhesive, the inner boundary is fixed and the expression is

$$u|_{r=r_1} = 0, \tag{12}$$

where r_1 represents the inner boundary of the coil. For case 2, when the coil is wound directly on the inner support structure, the inner boundary is free and thus

$$\sigma_r|_{r=r_1} = 0. \tag{13}$$

For case 1, the strain and stress profiles calculated for the 60-turn coil are shown in figure 8. When the heater is on, the turns near the heater expand along the radial direction and there is an obvious increase in radial strain. Due to the slow heat propagation velocity in the HTS, the outer turns experience a small compressive strain in the radial direction. Radial thermal expansion occurs in all turns as the temperature rises in the outer turns. When the temperature in all the turns decreases, the radial strain starts to reduce and finally becomes zero. However, the hoop strain shows a different trend at the initial stage. Because of the radial thermal expansion of the inner turns, all the turns in the coil experience tensile strain in the circumferential direction with the increase of the temperature. Although the temperature in the outer turns hardly changes, the deformation of the inner turns has an effect on the outer turns. With the rapid decrease of temperature in the inner turns, the hoop strain also reduces. For the stress, the radial stress is mainly positive or tensile. The reason is that we have fixed the displacement of the inner

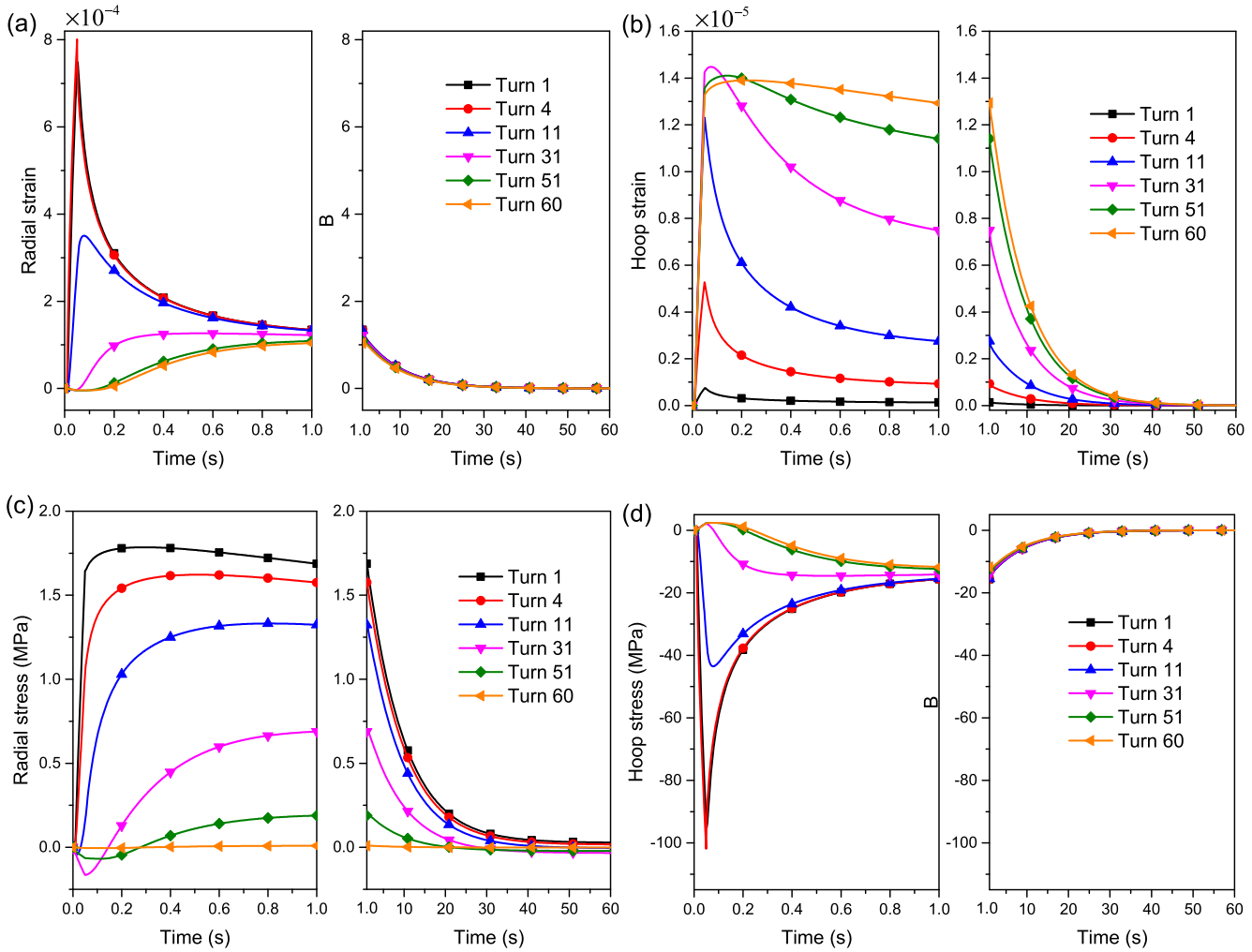

Figure 8. Distributions of radial strain (a), hoop strain (b), radial stress (c) and hoop stress (d) in the 60-turn coil with a fixed inner boundary.

boundary. The radial stress in the coil reduces with the decrease of temperature, but cannot return to zero because of the effect of electromagnetic force. It can also be seen that the electromagnetic force has a small effect on the radial stress in the self-field. Furthermore, the hoop stress is larger than the radial stress in the coil, which means that the coil is mainly subjected to hoop stress during the heating and recovery processes. The radial expansion leads to relative compression along the circumferential direction during heating. However, the hoop stress almost vanishes when the temperature returns to the initial value. This also indicates that the electromagnetic force has little effect on the mechanical behavior in the self-field.

For case 2, figure 9 shows the distributions of strain and stress in the 60-turn coil, respectively. During heating, the inner turns expand in the radial direction as the temperature increases, while the temperature of the outer turns does not change because of the slow heat propagation velocity. Because the inner boundary is free, the outer turns experience a larger compressive strain than in case 1. When the temperature of the outer turns rises, the change of the radial strain follows the same trend as in case 1. However, the hoop strain shows a significant difference compared with case 1. The reason is that the thermal expansion in the radial direction is free at the inner boundary. Meanwhile, the outer turns because of a slow heat propagation velocity are mainly affected by the deformation of the inner turns, which explains why the coil experiences a large tensile strain in the hoop direction. When the temperature of the inner turns rapidly decreases, the hoop strain also reduces. The radial stress is mainly negative or compressive. This is because the free expansion leads to extrusion deformation among the turns, resulting from the effect of the free inner boundary. However, as the temperature of the inner turns rises during heating, their expansion leads to the relative compression of the inner turns in the circumferential direction. Meanwhile, the expansion of the inner turns is limited by the outer turns, which are stretched in the circumferential direction. It can also be seen that the electromagnetic force has little effect on the mechanical behavior in the self-field for case 2. Moreover, the change in the hoop stress is larger than the change in the radial stress. Note that the free inner boundary is used in the following.

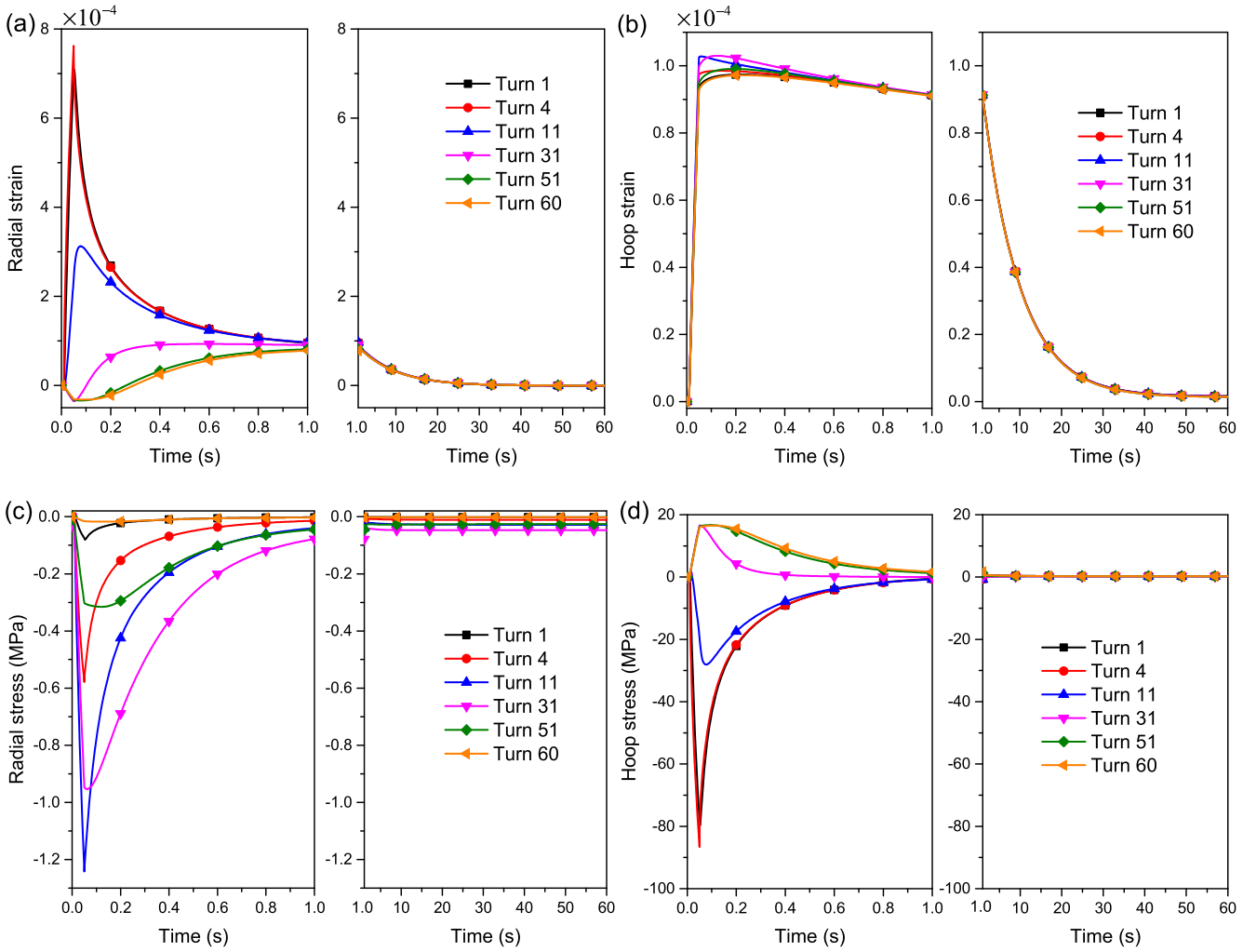

Figure 9. Distributions of radial strain (a), hoop strain (b), radial stress (c) and hoop stress (d) in the 60-turn coil with the free inner boundary.

4. Discussions

4.1. Effect of pulsed energy

When the pulsed energy of the heater is raised, the temperature profile of the 60-turn coil is as shown in figure 10. It shows that the same turn experiences a larger temperature rise when a high pulsed energy is applied, and the coil needs a longer time to recover. Moreover, more of the inner turns in the coil exceed the critical temperature during heating. Thus, the current in the inner turns flow in the radial direction, and the outer turns are mainly circumferential current along the superconducting layer. The central field determined by the circumferential current of the coil has a large reduction and the coil voltage determined by the radial current has a large increase, as shown in figure 11. At the end of the heat pulse, the turn nearest the temperature propagation front experiences a larger radial compressive stress than the other turns, as shown in figure 12. Turn 1 has a small compressive stress because of the free inner boundary. Since turn 60 is far away from the area where the temperature is rising, the radial stress is very small. The location of the temperature front is different for different pulsed energies, which leads to a difference in

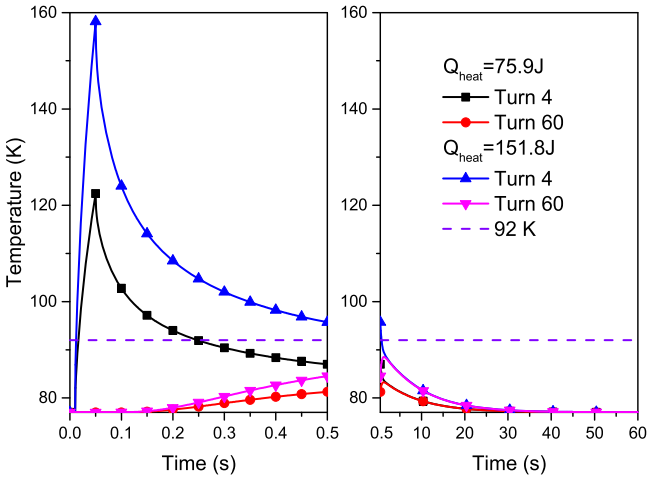

Figure 10. Effect of the different pulsed energies on the thermal stability in the 60-turn coil.

the location of the maximum radial stress. As for the hoop stress, turn 4 has the largest compressive hoop stress because it experiences the largest temperature rise. The outer turns limit the expansion of the inner turns and they have relatively

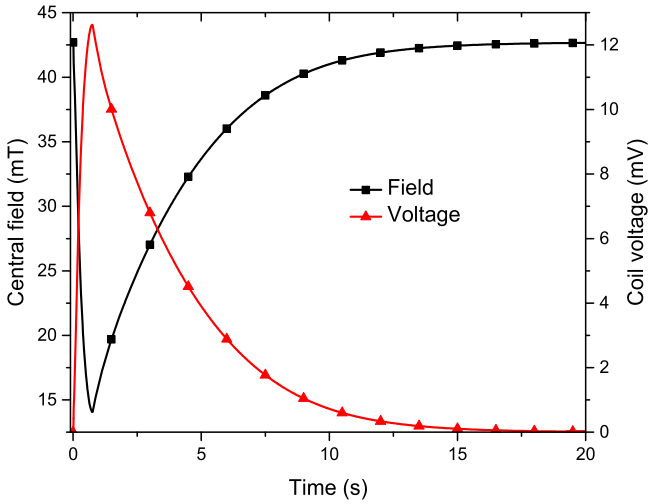

Figure 11. Central field and voltage with the pulsed energy of 151.8 J in the 60-turn coil.

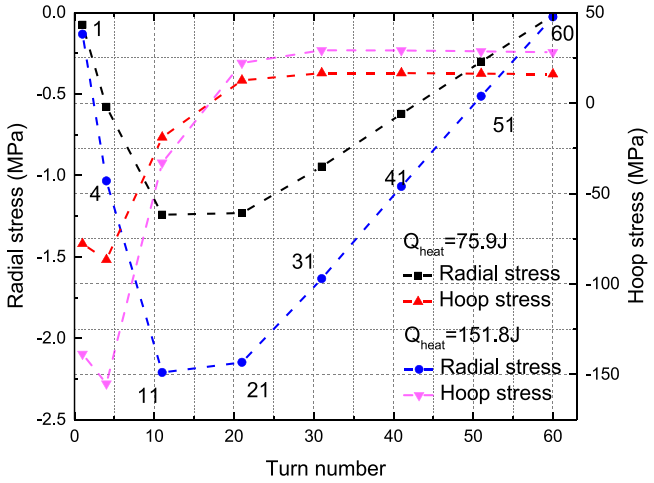

Figure 12. Radial and hoop stresses with different pulsed energies at the end of the heat pulse (50 ms).

small tensile hoop stress. With an increase of pulsed energy, the radial and hoop stresses have an obvious increase. Furthermore, the change in hoop stress is larger than the change in radial stress. In other words, hoop stress dominates the mechanical stability during local heat disturbance.

4.2. Effect of inner diameter

For the coil with a smaller inner diameter for a pulsed energy of 75.9 J, the temperature rise in the same turn is higher, as shown in figure 13. The reason is that the length of turn 4 is shorter for a coil with a small inner diameter, so that the per unit volume energy increases for the heater with the same energy. Figure 14 shows the central field and voltage for the 60-turn coil with an inner diameter of 40 mm. Because the power supply current stays unchanged, a coil with a small inner diameter has a larger central field. Because of the higher per unit volume energy, the central field has a larger decrease and the coil voltage has a larger increase after heating. The

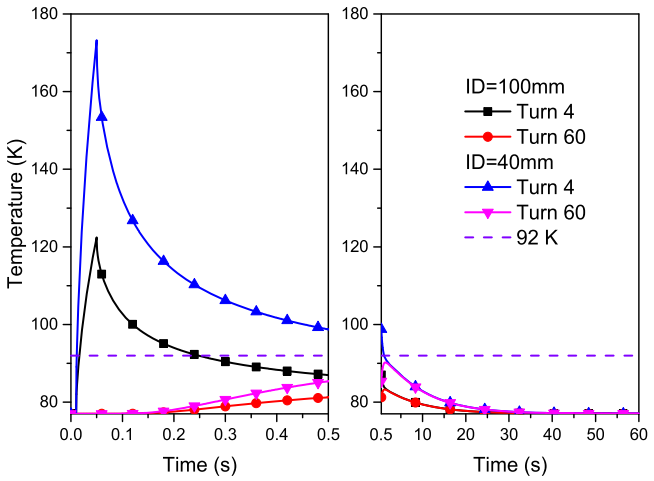

Figure 13. Effect of the different inner diameters on the thermal stability in the 60-turn coil.

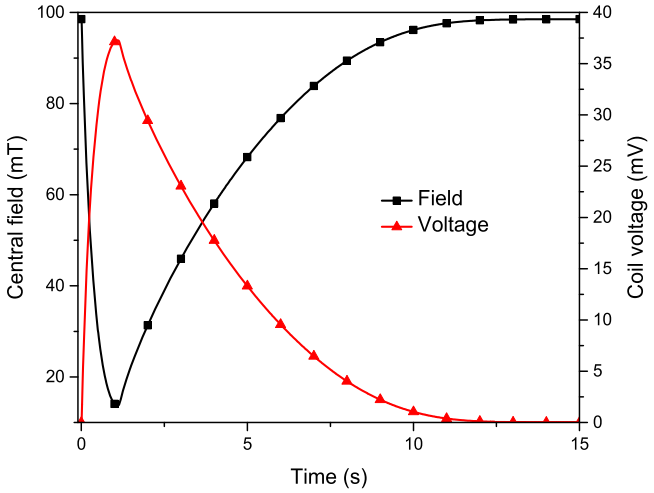

Figure 14. Central field and voltage with the inner diameter of 40 mm in the 60-turn coil.

distributions of radial and hoop stresses at the end of the heat

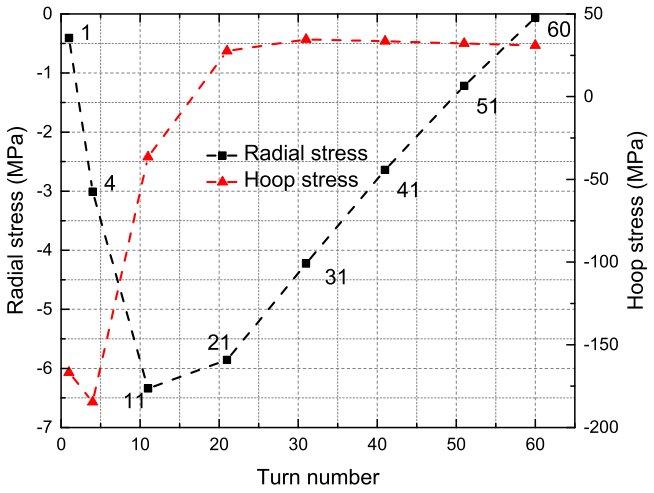

Figure 15. Radial and hoop stresses with the inner diameter of 40 mm at the end of the heat pulse (50 ms).

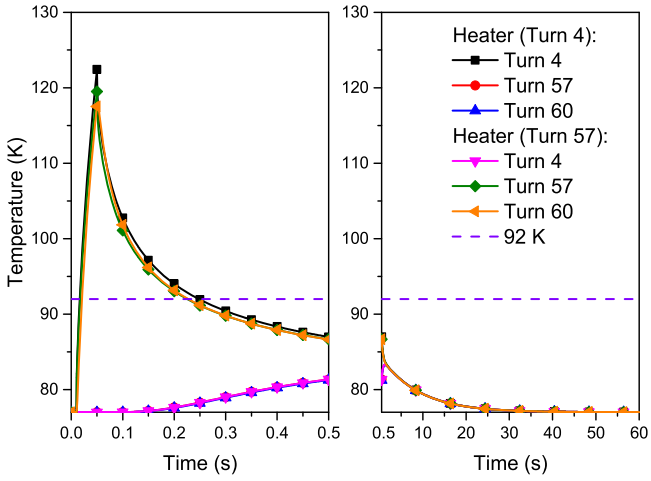

Figure 16. Effect of the location of the heater on the thermal stability in the 60-turn coil. Heaters are located in turn 4 and turn 57, respectively.

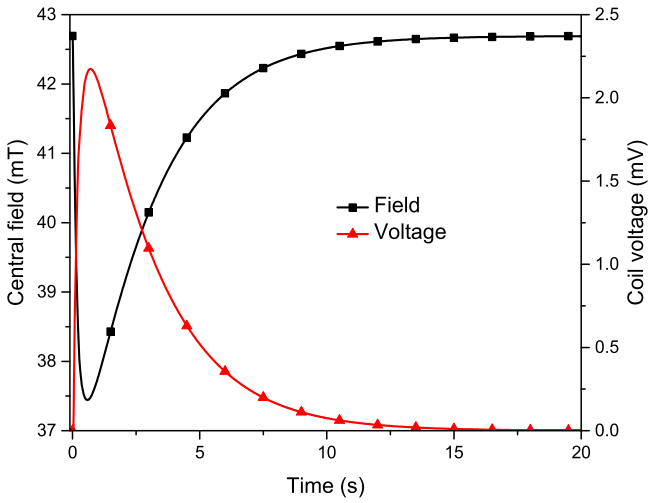

Figure 17. Central field and voltage with the heater located in turn 57 in the 60-turn coil.

pulse are shown in figure 15. Compared with the coil with a large inner diameter, the radial stress in turn 60 is still smaller and the location of the temperature propagation front is different, thus the location of the largest radial stress is also different. Due to the increase of the temperature rise in the inner turns for the coil with a small inner diameter, the hoop stress increases in all turns.

4.3. Effect of location of the heater

When the location of the heater is moved to turn 57, the temperature profile of the coil is as shown in figure 16. For the same energy, the longer length of turn 57 leads to a decrease of per unit volume energy and thus the largest temperature rise is also smaller. Fewer of the inner turns exceed the critical temperature, resulting in a small reduction in the central field and a small increase in the coil voltage, as shown in figure 17. Figure 18 shows the changes of the radial and hoop stresses at the end of the heat pulse with the heater

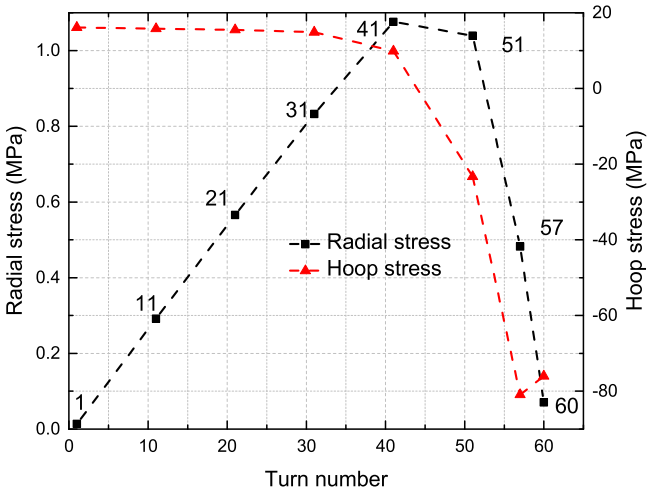

Figure 18. Radial and hoop stresses with the heater located in turn 57 at the end of the heat pulse (50 ms).

in turn 57. However, the radial stress is positive or tensile in all turns in this case. The reason is that the thermal expansion occurs first in the outer turns with the heater located in turn 57. Thus, the coil is stretched outwards along the radial direction. Moreover, the location of the temperature propagation front still determines the location of the largest radial stress. Turn 1 is far away from the heater and thus the radial stress is small. The hoop stress reaches a maximum for the largest temperature rise in turn 57. The inner turns limit the expansion of the outer turns, which shows the opposite change trend to the case when the heater is located in turn 4. Moreover, the change of hoop stress is still larger than the change of the radial stress.

5. Conclusions

In this paper, a multiphysics quench model combining an equivalent circuit axisymmetric model with a 2D magnetic field model and 1D heat transfer model is built to study the quench mechanism of the NI coil. The mechanical characteristics are also investigated in the quench and recovery processes. When the temperature of the coil is more than the critical value, the current flows in the radial direction. The heat generated by the radial resistance is small, so that the coil has a higher thermal stability. For the different inner boundaries, the change of the strain and stress has a different trend. However, the change of hoop stress is larger than the change of radial stress. The distributions of strain and stress are mainly affected by thermal expansion and heat propagation velocity with the electromagnetic force having little effect on both cases. The maximum radial stress is dependent on the location of the temperature propagation front at the end of the heat pulse and the largest hoop stress appears in the turn experiencing the largest temperature rise. When the pulsed energy, inner diameter of the coil and location of the heater change, they all have observable effects on the thermal stability and mechanical behavior of the NI coils.

Acknowledgments

The authors acknowledge the support from the National Natural Science Foundation of China (Nos. 11327802 and 11472120), 111 Project (B14044) and the Fundamental Research Funds for the Central Universities (lzujbky-2017-it61 and lzujbky-2017-k18). The authors also thank Michael Luetchford, BTech, from Liwen Bianji, Edanz Group China (www.liwenbianji.cn/ac), for editing the English text of a draft of this manuscript.

ORCID iDs

Huadong Yong https://orcid.org/0000-0002-0304-3191

References

[1] Weijers H W *et al* 2014 Progress in the development of a superconducting 32 T magnet with REBCO high field coils *IEEE Trans. Appl. Supercond.* **24** 4301805
[2] Senatore C, Alessandrini M, Lucarelli A, Tediosi R, Uglietti D and Iwasa Y 2014 Progresses and challenges in the development of high-field solenoidal magnets based on RE123 coated conductors *Supercond. Sci. Technol.* **27** 103001
[3] Xia J, Bai H, Lu J, Gavrilin A V, Zhou Y and Weijers H W 2015 Electromagnetic modeling of REBCO high field coils by the H-formulation *Supercond. Sci. Technol.* **28** 125004
[4] Rossi L 2016 Toward a new paradigm in quench detection for superconducting magnets? 'Quench detection for high temperature superconductor magnets: a novel technique based on Rayleigh-backscattering interrogated optical fibers (RIOF)' *Supercond. Sci. Technol.* **29** 060501
[5] Lacroix C, Lapierre Y, Coulombe J and Sirois F 2014 High normal zone propagation velocity in second generation high-temperature superconductor coated conductors with a current flow diverter architecture *Supercond. Sci. Technol.* **27** 055013
[6] Kim H, Kwon Y, Lee J, Song J and Lee H 2009 Quench and recovery characteristics of a racetrack double pancake coil wound with YBCO-coated conductor *Supercond. Sci. Technol.* **22** 025014
[7] Chan W, Flanagan G and Schwartz J 2013 Spatial and temporal resolution requirements for quench detection in (RE)$Ba_2Cu_3O_x$ magnets using Rayleigh-scattering-based fiber optic distributed sensing *Supercond. Sci. Technol.* **26** 105015
[8] Liu W, Yong H and Zhou Y 2016 Numerical analysis of quench in coated conductors with defects *AIP Adv.* **6** 095023
[9] Hahn S, Park D K, Bascuñán J and Iwasa Y 2011 HTS pancake coils without turn-to-turn insulation *IEEE Trans. Appl. Supercond.* **21** 1592–5
[10] Wang T *et al* 2015 Analyses of transient behaviors of no-insulation REBCO pancake coils during sudden discharging and overcurrent *IEEE Trans. Appl. Supercond.* **25** 4603409
[11] Hahn S *et al* 2016 'Defect-irrelevant' behavior of a no-insulation pancake coil wound with REBCO tapes containing multiple defects *Supercond. Sci. Technol.* **29** 105017
[12] Wang Y, Chan W K and Schwartz J 2016 Self-protection mechanisms in no-insulation (RE) $Ba_2Cu_3O_x$ high temperature superconductor pancake coils *Supercond. Sci. Technol.* **29** 045007
[13] Wang X *et al* 2013 Turn-to-turn contact characteristics for an equivalent circuit model of no-insulation ReBCO pancake coil *Supercond. Sci. Technol.* **26** 035012
[14] Hahn S *et al* 2013 No-insulation multi-width winding technique for high temperature superconducting magnet *Appl. Phys. Lett.* **103** 173511
[15] Song J-B, Hahn S, Lécrevisse T, Voccio J, Bascuñán J and Iwasa Y 2015 Over-current quench test and self-protecting behavior of a 7 T/78 mm multi-width no-insulation REBCO magnet at 4.2 K *Supercond. Sci. Technol.* **28** 114001
[16] Lee T S *et al* 2014 The effects of co-wound Kapton, stainless steel and copper, in comparison with no insulation, on the time constant and stability of GdBCO pancake coils *Supercond. Sci. Technol.* **27** 065018
[17] Schwartz J 2016 Are no-insulation magnets a paradigm shift for high-field DC superconducting magnets? *Supercond. Sci. Technol.* **29** 050501
[18] Song H and Wang Y 2016 Simulations of nonuniform behaviors of multiple no-insulation (RE)$Ba_2Cu_3O_{7-x}$ HTS pancake coils during charging and discharging *IEEE Trans. Appl. Supercond.* **26** 4700105
[19] Kim J *et al* 2016 Effect of resistive metal cladding of HTS tape on the characteristic of no-insulation coil *IEEE Trans. Appl. Supercond.* **26** 4601906
[20] Kim K *et al* 2017 Quench behavior of a no-insulation coil wound with stainless steel cladding REBCO tape at 4.2 K *Supercond. Sci. Technol.* **30** 075001
[21] Yanagisawa Y *et al* 2014 Basic mechanism of self-healing from thermal runaway for uninsulated REBCO pancake coils *Physica* C **499** 40–4
[22] Choi Y, Hahn S, Song J, Yang D and Lee H 2011 Partial insulation of GdBCO single pancake coils for protection-free HTS power applications *Supercond. Sci. Technol.* **24** 125013
[23] Oki T *et al* 2016 Evaluation on quench protection for no-insulation REBCO pancake coil *IEEE Trans. Appl. Supercond.* **26** 4702905
[24] Choi Y H *et al* 2014 Thermal quench behaviors of no-insulation coils wound using GdBCO coated conductor tapes with various lamination materials *IEEE Trans. Appl. Supercond.* **24** 8800105
[25] Jang J Y *et al* 2017 Design, construction and 13 K conduction-cooled operation of a 3 T 100 mm stainless steel cladding all-REBCO magnet *Supercond. Sci. Technol.* **30** 105012
[26] Wang Y, Song H, Xu D, Li Z, Jin Z and Hong Z 2015 An equivalent circuit grid model for no-insulation HTS pancake coils *Supercond. Sci. Technol.* **28** 045017
[27] Kim S, Hahn S, Kim K and Larbalestier D 2017 Method for generating linear current-field characteristics and eliminating charging delay in no-insulation superconducting magnets *Supercond. Sci. Technol.* **30** 035020
[28] Suetomi Y, Yanagisawa K, Nakagome H, Hamada M, Maeda H and Yanagisawa Y 2016 Mechanism of notable difference in the field delay times of no-insulation layer-wound and pancake-wound REBCO coils *Supercond. Sci. Technol.* **29** 105002
[29] Liu D, Yong H and Zhou Y 2017 Analysis of charging and sudden-discharging characteristics of no-insulation REBCO coil using an electromagnetic coupling model *AIP Adv.* **7** 115104
[30] Kim K L *et al* 2014 Effect of winding tension on electrical behaviors of a no-insulation ReBCO pancake coil *IEEE Trans. Appl. Supercond.* **24** 4600605
[31] Tong Y, Guan M and Wang X 2017 Theoretical estimation of quench occurrence and propagation based on generalized thermoelasticity for LTS/HTS tapes triggered by a spot heater *Supercond. Sci. Technol.* **30** 045002
[32] Wang X, Guan M and Ma L 2012 Strain-based quench detection for a solenoid superconducting magnet *Supercond. Sci. Technol.* **25** 095009

[33] Chan W K and Schwartz J 2017 Improved stability, magnetic field preservation and recovery speed in (RE) $Ba_2Cu_3O_x$-based no-insulation magnets via a graded-resistance approach *Supercond. Sci. Technol.* **30** 074007

[34] Chan W K, Masson P J, Luongo C and Schwartz J 2010 Three-dimensional micrometer-scale modeling of quenching in high-aspect-ratio $YBa_2Cu_3O_{7-\delta}$ coated conductor tapes—part I: model development and validation *IEEE Trans. Appl. Supercond.* **20** 2370–80

[35] Chan W K, Masson P J, Luongo C A and Schwartz J 2009 Influence of inter-layer contact resistances on quench propagation in $YBa_2Cu_3O_x$ coated conductors *IEEE Trans. Appl. Supercond.* **19** 2490–5

[36] Grilli F, Sirois F, Zermeno V M and Vojenčiak M 2014 Self-consistent modeling of the I_c of HTS devices: how accurate do models really need to be? *IEEE Trans. Appl. Supercond.* **24** 8000508

[37] Pelegrin J, Young E and Yang Y 2015 Numerical winding model for the analysis of superconducting insert coils *IEEE Trans. Appl. Supercond.* **25** 4900705

[38] Yoon S, Kim J, Cheon K, Lee H, Hahn S and Moon S 2016 26 T 35 mm all-$GdBa_2Cu_3O_{7-x}$ multi-width no-insulation superconducting magnet *Supercond. Sci. Technol.* **29** 04LT04

[39] Berger K, Lévêque J, Netter D, Douine B and Rezzoug A 2007 Influence of temperature and/or field dependences of the *E-J* power law on trapped magnetic field in bulk YBaCuO *IEEE Trans. Appl. Supercond.* **17** 3028–31

[40] Beyer R P and LeVeque R J 1992 Analysis of a one-dimensional model for the immersed boundary method *SIAM J. Numer. Anal.* **29** 332–64

[41] Wu H, Yong H and Zhou Y H 2018 Stress analysis in high temperature superconductors under pulsed field magnetization *Supercond. Sci. Technol.* **31** 045008

[42] Shin H-S and Dedicatoria M J 2012 Variation of the strain effect on the critical current due to external lamination in REBCO coated conductors *Supercond. Sci. Technol.* **25** 054013

[43] Wang X *et al* 2014 Numerical structural analysis on a new stress control structure for high-strength REBCO pancake coil *IEEE Trans. Appl. Supercond.* **24** 4601605